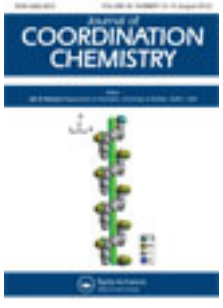

Journal of Coordination Chemistry
Publication details, including instructions for authors and subscription information:
http://www.tandfonline.com/loi/gcoo20

Synthesis, crystal structure, and magnetic properties of single end-to-end azido-bridged 1-D chain coordination polymers of Cu(II)

Ahmad Husain [a b], Mark M. Turnbull [c], Shahab A.A. Nami [d], A. Moheman [a] & K.S. Siddiqi [a b]

[a] Department of Chemistry, Aligarh Muslim University, Aligarh, Uttar Pradesh, India

[b] Department of Chemistry, Centre for Supramolecular Chemistry Research, University of Cape Town, Cape Town, South Africa

[c] Carlson School of Chemistry and Biochemistry, Clark University, Worcester, MA, USA

[d] Department of Kulliyat, Faculty of Unani Medicine, Aligarh Muslim University, Aligarh, Uttar Pradesh, India

Accepted author version posted online: 06 Jun 2012.Published online: 18 Jun 2012.

To cite this article: Ahmad Husain, Mark M. Turnbull, Shahab A.A. Nami, A. Moheman & K.S. Siddiqi (2012) Synthesis, crystal structure, and magnetic properties of single end-to-end azido-bridged 1-D chain coordination polymers of Cu(II), Journal of Coordination Chemistry, 65:15, 2593-2611, DOI: 10.1080/00958972.2012.700479

To link to this article: http://dx.doi.org/10.1080/00958972.2012.700479

Journal of Coordination Chemistry
Vol. 65, No. 15, 10 August 2012, 2593–2611

Synthesis, crystal structure, and magnetic properties of single end-to-end azido-bridged 1-D chain coordination polymers of Cu(II)

AHMAD HUSAIN†‡, MARK M. TURNBULL§, SHAHAB A.A. NAMI¶, A. MOHEMAN† and K.S. SIDDIQI*†‡

†Department of Chemistry, Aligarh Muslim University, Aligarh, Uttar Pradesh, India
‡Department of Chemistry, Centre for Supramolecular Chemistry Research, University of Cape Town, Cape Town, South Africa
§Carlson School of Chemistry and Biochemistry, Clark University, Worcester, MA, USA
¶Department of Kulliyat, Faculty of Unani Medicine, Aligarh Muslim University, Aligarh, Uttar Pradesh, India

(*Received 1 December 2011; in final form 19 April 2012*)

The synthesis and spectroscopic characterization of azido derivatives of Cu(II) complexes with macrocyclic building blocks of the type $[CuLN_3]_n \cdot [ClO_4 \cdot 3/2H_2O]_n$ (**1**), $[CuL(N_3)_2]$ (**2**) and $[CuL^1N_3]_n \cdot [ClO_4]_n$ (**3**) (where L = 3,10-bisbenzyl-1,3,5,8,10,12-hexaazacyclotetradecane and L^1 = 3,10-bisbenzyl-6,13-dimethyl-1,3,5,8,10,12-hexaazacyclotetradecane) are reported. On the basis of single-crystal X-ray diffraction, **1** and **3** have a 1-D polymeric chain where Cu(II) ions are bridged by single azide in the μ-1,3 (end-to-end) bridging mode in a *trans*-position with respect to the azide. When $[CuLN_3]_n \cdot [ClO_4 \cdot 3/2H_2O]_n$ was recrystallized from acetone, the non-polymeric **2** was obtained, where Cu(II) is in a tetragonally distorted octahedral environment. The chains of $[CuLN_3]_n \cdot [ClO_4 \cdot 3/2H_2O]_n$ and $[CuL^1N_3]_n \cdot [ClO_4]_n$ propagate parallel to the crystallographic *b*-axis and are stacked one over the other along the *c*-axis by hydrogen bonding. The azides exhibit symmetric coordination. The ClO_4^- ions fill channels formed between the strings of octahedra and are held in place by hydrogen bonds leading to the formation of a 3-D network. Compound **1** exhibits only very weak antiferromagnetic interactions, while **2** and **3** show no signs of magnetic exchange.

Keywords: Crystal structure; Cu(II) Macrocycle; 1-D Coordination polymer; Magnetism; Antiferromagnetic interactions; Azide ligands

1. Introduction

Construction of coordination polymers is rapidly growing because of fascinating structural motifs and potential applications as functional materials [1, 2]. Metal-organic complexes containing bridging ligands may be designed with specific functionalities [3–5]. The strategy for designing these molecular materials is to use suitable bridging ligands. Owing to versatile coordination modes and wide range of magnetic couplings,

*Corresponding author. Email: ahmad.chem786@hotmail.com; ks_siddiqi@yahoo.co.in

ISSN 0095-8972 print/ISSN 1029-0389 online
http://dx.doi.org/10.1080/00958972.2012.700479

azide has become one of the most extensively studied building blocks [6–8] enriching the stereochemistry of transition metal ions and also their spectroscopic properties. A major obstacle to a more comprehensive study of such azide-based polymeric coordination complexes is the lack of rational synthetic procedures, since with the present state of knowledge it is not possible to predict which coordination mode will be adopted by azide [9–11].

Azide is an efficient ligand for building diverse structural patterns as part of 1-, 2- or 3-D extended arrays or dinuclear complexes, and for being able to predict magnetic properties depending on the binding mode (scheme 1). The end-on mode provides a ferromagnetic interaction and the end-to-end mode mediates antiferromagnetic exchange [12]. Numerous relevant systems exhibit various properties [13–19]. 1-D chain compounds with a linear or zigzag geometry are of interest in magnetochemistry and condensed matter physics due to the possibility of generating Haldane gap-type systems and single-chain magnets [20–22].

We reported two new polyaza-macrocyclic ligands L and L^1 and Cu(II) complexes with various counter ions and explored the consequence of anion coordination [23, 24]. In this work, we report syntheses, structures and magnetic properties of azide-bridged, 1-D infinite chain Cu(II) complexes with mononucleating 14-membered hexaazamacrocyclic ligands L and L^1 (L = 3,10-bisbenzyl-1,3,5,8,10,12-hexaazacyclotetradecane

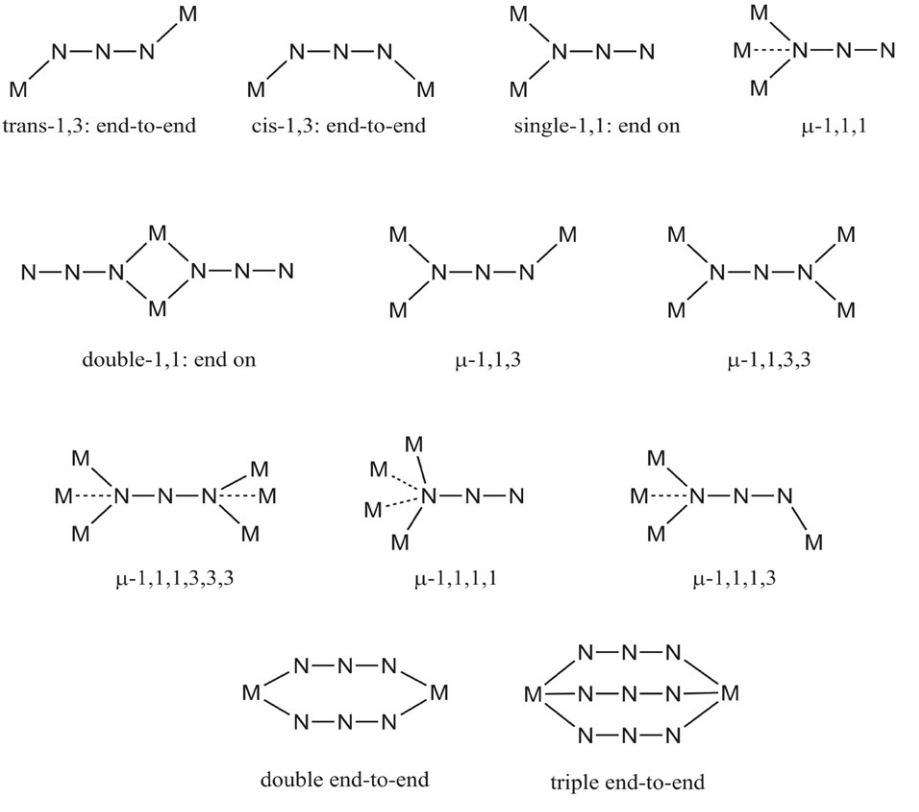

Scheme 1. Different binding modes of azide ligand.

and $L^1 = 3,10$-bisbenzyl-6,13-dimethyl-1,3,5,8,10,12-hexaazacyclotetradecane). In **1** and **3**, ClO_4^- occupies voids in the lattice for charge compensation and the Cu(II) centers are bridged by azide end-to-end.

2. Experimental

2.1. *Material and methods*

$Cu(CH_3COO)_2 \cdot H_2O$, $HClO_4$ (Merck India), ethylenediamine, 1,2-diaminopropane, NaN_3 (E. Merck), benzylamine, and formaldehyde (S.D. Fine India) were used as received. Methanol and ethanol were distilled prior to use. Elemental analyses were done with a FLASH EA 1112 SERIES CHNS analyzer. IR spectra (4000–400 cm^{-1}) were recorded with a Spectrolab Interspec FT/IR–2020 spectrometer as KBr discs. Conductivity measurements were carried out with a CM-82T Elico conductivity bridge in acetonitrile. EPR spectra were recorded in the solid state and in frozen CH_3CN/toluene with a JEOL FE3X EPR spectrometer at X-band microwave frequency. Powder XRD patterns of all samples were recorded with a Bruker-AXS, D8 Advance diffractometer using Cu-Kα X-radiation at 35 kV and 25 mA. Diffraction patterns were collected over 2θ range of 5–50° at a scan rate of 1°min^{-1}.

Caution! Although our samples never exploded during handling, perchlorate and azide metal complexes are potentially explosive and should be handled with care.

2.2. *Synthesis of $[CuL](ClO_4)_2$ and $[CuL^1](ClO_4)_2$*

$[CuL](ClO_4)_2$ and $[CuL^1](ClO_4)_2$ were synthesized as reported [23, 24].

2.3. *Synthesis of $[CuLN_3]_n \cdot [ClO_4 \cdot 3/2H_2O]_n$ (1) [(L = 3,10-bisbenzyl-1,3,5,8,10,12-hexaazacyclotetradecane)]*

To an acetonitrile (20 mL) solution of $[CuL](ClO_4)_2$ [23] (1 mmol L^{-1}, 0.645 g) an excess of sodium azide (two-fold excess) was added and stirred for 1 h. The mixture was filtered to remove solid $NaClO_4$ and the solvent was evaporated to dryness to give a blue-violet powder. The powder was dissolved in acetonitrile and a few drops of water was added and allowed to stand at room temperature. Violet needles were obtained after 15 days, collected by filtration, and washed with ethanol. Yield: ~93% (0.57 g). m.p.: 200°C. Anal. Calcd for $C_{22}H_{34}CuN_9ClO_{5.5}$ (**1**): C, 43.21; H, 5.60; N, 20.61. Found: C, 44.01; H, 5.79; N, 20.33. IR (KBr, cm^{-1}): 3243, 3173, 2926, 2872, 2063, 1447, 1418, 1377, 1269, 1111, 1086, 997, 934, 855, 744, 696, 627, 440.

2.4. *Synthesis of $[CuL(N_3)_2]$ (2) [(L = 3,10-bisbenzyl-1,3,5,8,10,12-hexaazacyclo-tetradecane)]*

Complex **1** (0.61 g) was dissolved in acetone and filtered. The filtrate was allowed to stand at room temperature giving blue pellets after 7 days. Yield: ~85% (0.45 g).

m.p.: 206°C. Anal. Calcd for $C_{22}H_{34}CuN_{12}$ (**2**): C, 49.84; H, 6.46; N, 31.71. Found: C, 50.07; H, 6.89; N, 31.43. IR (KBr, cm^{-1}): 3129, 2932, 2875, 2020, 1463, 1422, 1380, 1272, 858, 741, 696, 418.

2.5. *Synthesis of $[CuL^1N_3]_n \cdot [ClO_4]_n$ (3) [(L^1 = 3,10-bisbenzyl-6, 13-dimethyl-1,3,5,8,10,12-hexaazacyclotetradecane)]*

To an acetonitrile (20 mL) solution of $[CuL^1](ClO_4)_2$ [24] (1 mmol, 0.673 g), excess of sodium azide (two-fold excess) was added and stirred for 10 min. The solution was filtered to remove solid $NaClO_4$ and allowed to stand for a few days yielding blue-violet blocks, which were collected by filtration and washed with ethanol. Yield: ~90% (0.68 g). m.p.: 191°C. Anal. Calcd for $C_{24}H_{38}CuN_9ClO_4$ (**3**): C, 46.82; H, 6.22; N, 20.48. Found: C, 47.09; H, 6.10; N, 21.00%. IR (KBr, cm^{-1}): 3230, 2932, 2053, 1456, 1259, 1108, 1089, 1032, 981, 744, 696, 627, 418.

2.6. *X-ray crystal structure determination and refinements*

X-ray data for **1** was collected on a Bruker SMART APEX CCD diffractometer at 100(2) K. SMART [25] was used for collecting frames of data, indexing reflections, and determining lattice parameters. The data integration and reduction were processed with SAINT [25]. An empirical absorption correction was applied to the collected reflections with SADABS [26] using XPREP [27]. X-ray data for **2** and **3** were collected on an Oxford Diffraction Gemini CCD equipped diffractometer at 298(2) K using graphite-monochromated Mo-Kα radiation ($\lambda = 0.71073$ Å). The strategy for the data collection was evaluated by the CrysAlisPro CCD program and collected by standard "phi-omega scan" techniques, scaled, and reduced using CrysAlisPro RED program [28]. Linear absorption coefficients, scattering factors for atoms, and anomalous dispersion corrections were taken from the International Tables for X-ray Crystallography [29]. The structure of **1** was solved by the Patterson method and those of **2** and **3** by direct methods using SHELXS-97 [30] and refined on F^2 by full-matrix least squares using SHELXL-97 [30]. All hydrogen atoms bonded to carbon were placed in calculated positions and refined isotropically while N–H hydrogen atoms were located in the difference Fourier maps, and refined with fixed isotropic U's, except the hydrogen of N(3) in **1**; we were unable to locate hydrogen on the water molecules. Figures were drawn using ORTEP-3.2 [31], MERCURY-2.3 [32], and DIAMOND-3.0 [33]. The pertinent crystal data and refinement parameters for **1**–**3** are compiled in table 1.

2.7. *Magnetic data collection*

Magnetic data were collected using a Quantum Design MPMS-XL SQUID magnetometer. Finely ground samples were placed in gelatin capsules and the magnetic moments were measured in magnetic fields of 0–50 kOe at 1.8 K. As the magnetic field was brought back to 0 kOe, several data points were collected to determine if there was hysteresis; none was observed. The temperature-dependent magnetic susceptibility data for each sample were collected over a temperature range of 1.8–310 K in an applied magnetic field of 1 kOe, within the linear range of M *versus* H response. All data sets

Table 1. Crystallographic data of **1**, **2**, and **3**.

	1	**2**	**3**
Complex	$[CuLN_3]_n \cdot [ClO_4 \cdot 3/2H_2O]_n$	$[CuL(N_3)_2]$	$[CuL^1N_3]_n \cdot [ClO_4]_n$
Empirical formula	$C_{44}H_{66}Cl_2Cu_2N_{18}O_{11}$	$C_{22}H_{34}CuN_{12}$	$C_{24}H_{38}ClCuN_9O_4$
Formula weight	1221.15	530.15	615.62
Temperature (K)	100(2)	298(2)	298(2)
Wavelength (Å)	0.71073	0.71073	0.71073
Crystal system	Monoclinic	Monoclinic	Triclinic
Space group	$C2/c$	$P2/1c$	$P\bar{1}$
Unit cell dimensions (Å, °)			
a	42.97(3)	10.193(2)	6.5896(9)
b	6.353(4)	16.040(3)	10.1015(13)
c	20.379(12)	7.685(3)	11.4283(18)
α	90	90	71.500(13)
β	101.582(19)	91.86(2)	82.487(12)
γ	90	90	81.241(11)
Volume (Å^3), Z	5450(6), 4	1255.7(5), 2	710.24(17), 1
Calculated density (g cm^{-3})	1.486	1.402	1.439
Absorption coefficient (mm^{-1})	0.952	0.906	0.910
$F(000)$	2544	558	323
Crystal size (mm^3)	$0.10 \times 0.20 \times 0.30$	$0.15 \times 0.10 \times 0.10$	$0.30 \times 0.15 \times 0.10$
θ range for data collection (°)	2.04–25.0	2.94–24.99	3.14–25.00
Limiting indices	$-38 \le h \le 50$; $-7 \le k \le 7$; $-23 \le l \le 24$	$-7 \le h \le 12$; $-11 \le k \le 19$; $-9 \le l \le 8$	$-7 \le h \le 7$; $-12 \le k \le 10$; $-12 \le l \le 13$
Reflections collected	13,328	4950	4747
Independent reflection	4792 [$R_{int} = 0.1043$]	2207 [$R_{int} = 0.0310$]	2492 [$R_{int} = 0.0268$]
Max. and min. transmission	0.9108 and 0.7633	0.9148 and 0.8761	0.9145 and 0.7719
Refinement method	Full-matrix least-squares on F^2	Full-matrix least-squares on F^2	Full-matrix least-squares on F^2
Data/restraints/parameters	4792/3/343	2207/1/168	2492/0/200
Goodness-of-fit on F^2	1.051	1.039	0.990
Final R indices [$I > 2\sigma(I)$]	$R_1 = 0.0954$, $wR_2 = 0.2569$[a]	$R_1 = 0.0342$, $wR_2 = 0.0837$[a]	$R_1 = 0.0414$, $wR_2 = 0.0929$[a]
R indices (all data)	$R_1 = 0.1325$, $wR_2 = 0.2970$	$wR_1 = 0.0499$, $wR_2 = 0.0878$	$R_1 = 0.0553$, $wR_2 = 0.0972$
Largest difference peak and hole (e Å^{-3})	1.829/−0.957	0.313/−0.333	0.378/−0.285
Completeness to $\theta = 25.00$ (%)	99.6	99.9	99.9

[a] $R_1 = [\Sigma(|F_o| - |F_c|)]/\Sigma|F_o|$; $wR_2 = [\Sigma[w(|F_o|^2 - |F_c|^2)^2]/\Sigma[w(|F_o|^2)^2]]^{1/2}$; $w = 1/[\sigma^2|F_o|^2 + (xp)^2]$, where $p = [|F_o|^2 + 2|F_c|^2]/3$; $x = 0.0605$.

were corrected for contribution of the sample holder (measured independently), the intrinsic diamagnetism of the constituent atoms (*via* Pascal's constants) [34], and the temperature-independent paramagnetism of Cu(II).

3. Results and discussion

3.1. *Crystal structure description of $[CuLN_3]_n \cdot [ClO_4 \cdot 3/2H_2O]_n$ (1)*

An ORTEP drawing of **1** with an atomic numbering scheme is shown in figure 1 and the crystallographic data, selected bond lengths and angles are listed in tables 1 and 2.

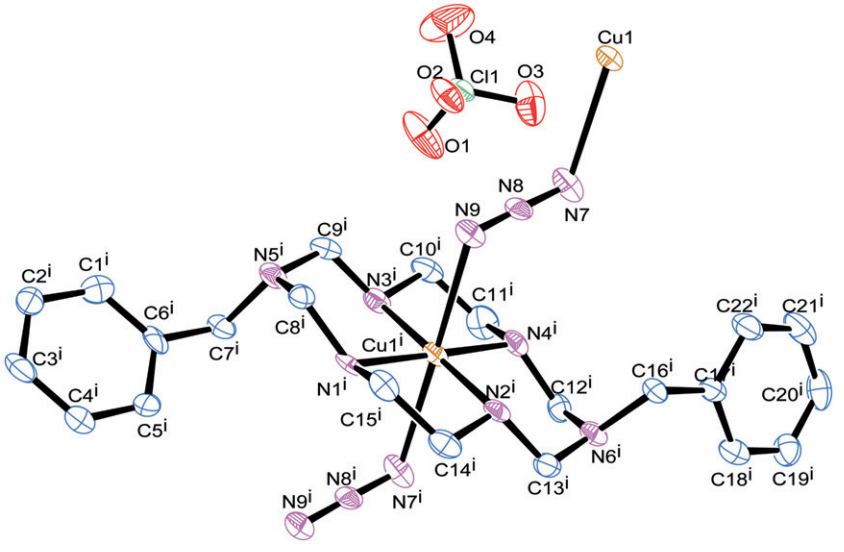

Figure 1. The molecular structure of **1** showing 30% probability displacement ellipsoids and atom-numbering scheme. Hydrogen atoms and lattice water molecules have been omitted for clarity.

Table 2. Bond lengths (Å) and angles (°) for **1**.

Bond lengths		Bond angles	
Cu(1)–N(1)	2.032(6)	N(2)–Cu(1)–N(9)	87.1(2)
Cu(1)–N(2)	2.032(6)	N(3)–Cu(1)–N(4)	86.2(3)
Cu(1)–N(3)	2.031(6)	N(3)–Cu(1)–N(7)	89.9(2)
Cu(1)–N(4)	2.026(6)	N(3)–Cu(1)–N(9)	92.8(2)
Cu(1)–N(7)	2.582(7)	N(4)–Cu(1)–N(7)	90.8(2)
Cu(1)–N(9)	2.625(7)	N(4)–Cu(1)–N(9)	93.3(2)
N(7)–N(8)	1.188(9)	N(7)–Cu(1)–N(9)	175.3(2)
N(8)–N(9)	1.176(9)	Cu(1)–N(7)–N(8)	110.5(5)
Cl(1)–O(1)	1.385(7)	Cu(1)–N(9)–N(8)#1	106.0(5)
Cl(1)–O(2)	1.454(6)	C(12)–N(6)–C(13)	116.8(6)
Cl(1)–O(3)	1.421(7)	C(12)–N(6)–C(16)	115.7(5)
Cl(1)–O(4)	1.420(9)	C(13)–N(6)–C(16)	116.3(6)
		C(9)–N(5)–C(8)	114.4(6)
Bond angles		C(9)–N(5)–C(7)	114.4(6)
N(1)–Cu(1)–N(2)	86.3(3)	C(8)–N(5)–C(7)	115.7(6)
N(1)–Cu(1)–N(3)	93.6(3)	N(9)–N(8)–N(7)	177.9(7)
N(1)–Cu(1)–N(4)	179.3(2)	O(1)–Cl(1)–O(4)	110.8(6)
N(1)–Cu(1)–N(7)	89.8(2)	O(1)–Cl(1)–O(3)	108.6(4)
N(1)–Cu(1)–N(9)	86.1(2)	O(4)–Cl(1)–O(3)	109.3(5)
N(2)–Cu(1)–N(3)	179.79(19)	O(1)–Cl(1)–O(2)	109.3(3)
N(2)–Cu(1)–N(4)	94.0(3)	O(4)–Cl(1)–O(2)	108.0(4)
N(2)–Cu(1)–N(7)	90.2(2)	O(3)–Cl(1)–O(2)	110.8(3)

Symmetry transformations used to generate equivalent atoms: #1: $x, -1:+y, z$.

$[CuLN_3]_n \cdot [ClO_4 \cdot 3/2H_2O]_n$ crystallizes in the monoclinic space group $C2/c$. The asymmetric unit of **1** consists of $[CuLN_3]^+$, one ClO_4^- and 3/2 water molecules. The octahedron around Cu(II) is achieved by four amine nitrogen atoms occupying the equatorial plane and two terminal nitrogen atoms of bridging azides at axial positions.

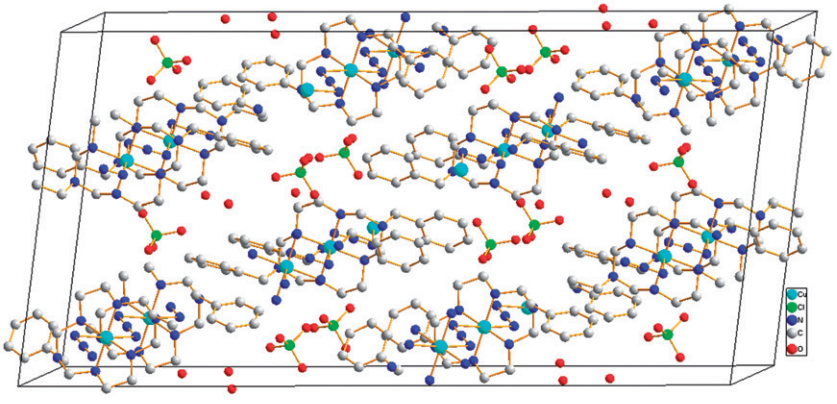

Figure 2. Unit cell diagram of **1** along the *b*-axis. Hydrogen atoms have been omitted for clarity.

The $[CuL]^{2+}$ units are connected by azide in the μ-1,3 (end-to-end) bridging mode that brings two neighboring metal centers into a *trans*-position with respect to the azide. This forms chains running parallel to the *b*-axis (figure 1), which belong to the type-I azido-bridged chain [35]. Equatorial Cu–N bond lengths are 2.025(6)–2.032(6) Å and *cis* N–Cu–N angles vary from 86.2(2)° to 93.2(2)° for five-membered and six-membered chelate rings. *Trans* N–Cu–N angles (179.2(2)° and 179.8(3)°) indicate that Cu(II) is slightly out of plane with some axial displacement; copper is 0.008 Å above the basal plane of N(1), N(2), N(3), and N(4), towards N(9), indicating different coordinating strength which is also evident from unequal Cu(1)–N(–N_3) bond lengths. The *EE* azide is linear within experimental error (angle N(9)–N(8)–N(7) of 177.9(7)°).

The observation of different N–N distances (1.188(9) and 1.177(9) Å), in agreement within the experimental error, suggests that it is symmetric bridging, not asymmetric [36]. The N–N–Cu angle is 110.4(5)° for the short Cu–N bond distance and 105.9(5)° for the longer one. Bond angles N(1–4)–Cu(1)–N(7) and N(1–4)–Cu(1)–N(9) are 86.10(2)–93.20(2)°, suggesting that Cu(1)–N(7) and Cu(1)–N(9) linkages are slightly bent off the perpendicular to the equatorial plane by 0.10–3.90°. The intrachain separation between the two neighboring copper atoms along the chain is 6.353 Å. Packing of the unit cell is provided in figure 2. Each chain of one sheet projects into holes of the next sheet in the superposition structure in a hexagonal close packing (A–B–A–B–···) arrangement (scheme 2).

Angles subtended at N(5) and N(6) are 114.4(6)–115.7(6)° and 115.7(5)–116.8(6)°, respectively [37]. The six-membered chelate rings involving C(8)/C(9) and C(12)/C(13) adopt a chair conformation with torsion angles of 57.66° and 55.24°, respectively, whereas the five-membered rings involving C(10)/C(11) and C(14)/C(15) assume a gauche conformation with torsion angles −56.02° and 55.99°, respectively. The *trans*-III configuration of the N-donors enables the hexaaza ring to adopt the least strained conformation. The torsion angle between planes of two benzene rings in two halves of the macrocycle is 159.73°, possibly due to intermolecular hydrogen bonding. The bond angles in perchlorate at Cl(1) are 108.0(4)–110.8(6)°, while bond distances vary from 1.39(6) to 1.454(5) Å.

The crystal structure exhibits different hydrogen bonding patterns (table 3). ClO_4^- and lattice water in the interchain spaces play a significant role in the hydrogen bonding

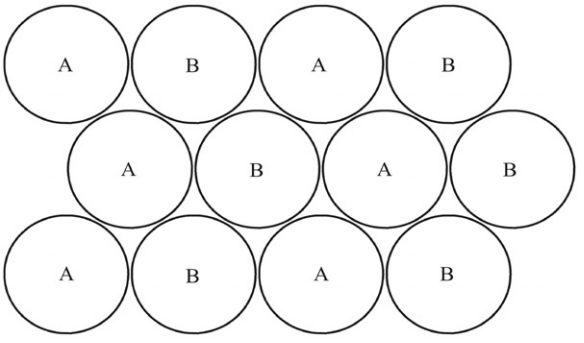

Scheme 2. Hexagonal close packing (A–B–A–B–···) arrangement of the sheets.

Table 3. Intramolecular and intermolecular hydrogen bonds, N–H···N, N–H···O and C–H···O, in **1**.

D–H–A	d(D···A) (Å)	d(H···A) (Å)	(D–H···A) (°)
N(1)–H(1N)···N(8) Intra	3.131(9)	2.56(5)	124(6)
N(2)–H(2N)···O(4)	2.891(11)	2.25(6)	130(4), x, $-1+y$, z
N(4)–H(4N)···N(8) Intra	3.194(9)	2.59(7)	127(7), x, $-1+y$, z
C(8)–H(8B)···N(9) Intra	3.254(10)	2.580	125.00
C(10)–H(10A)···O(2)	3.426(10)	2.580	143.00, x, $-y$, $1/2+z$
C(14)–H(14A)···O(4)	3.082(12)	2.470	120.00, x, $-1+y$, z

network. H(1N) is intramolecularly hydrogen bonded (figure 3) to N(8) of the azide. There is clearly a hydrogen bond between N3 and O2, even though the hydrogen on N(3) could not be located. The N–O distance of 3.012 is a strong indication and indicates the polar nature of the N–H bond. The shortest Cu–Cu distance between two H-bonded chains is 10.191 Å.

Crystal packing of **1** reveals that adjacent 1-D chains (figures 4 and 5) are linked by perchlorates *via* hydrogen bonds to give sheets. Those layers are stacked such that the benzyl groups are interleaved to minimize free volume which is responsible for the hexagonal close packing arrangement. An interesting feature of this complex is the joining of two parallel neighboring chains *via* hydrogen bonds formed by the perchlorate and lattice water to give a 3-D array. ClO_4^- is intimately involved in the hydrogen bond network of **1**, with three oxygen atoms engaged in N–H···O or C–H···O hydrogen bonds. The lattice water is held by water(lattice)···water(lattice) (O(5)···O(6) = 2.716 Å) hydrogen bonds (figure 4). The water oxygen (O6) is symmetrically disordered over two positions with respect to the two-fold rotational symmetry, each with 50% occupancy. None of the water protons could be located in difference Fourier maps and thus were not included in the final refinements.

3.2. *Crystal structure description of [CuL(N$_3$)$_2$] (2)*

The molecular structure of **2** with atom numbering scheme is shown in figure 6. Crystallographic data, selected bond lengths, and angles are given in tables 1 and 4.

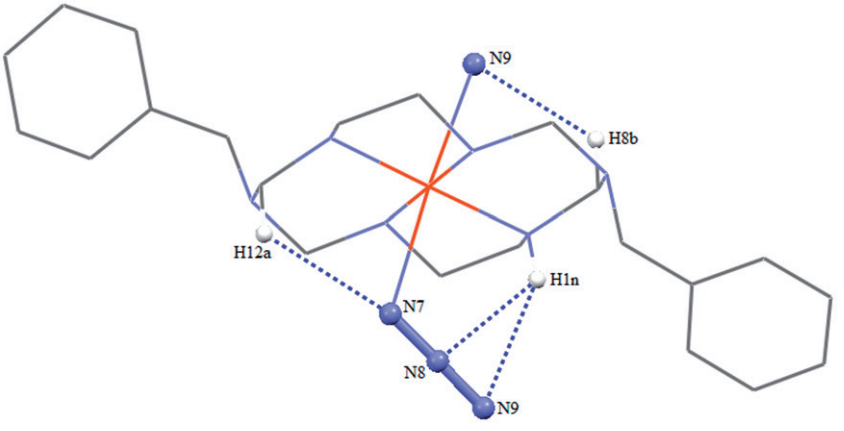

Figure 3. Intramolecular hydrogen bonding in **1**. H (white) and N (blue) are shown as small spheres of arbitrary radii.

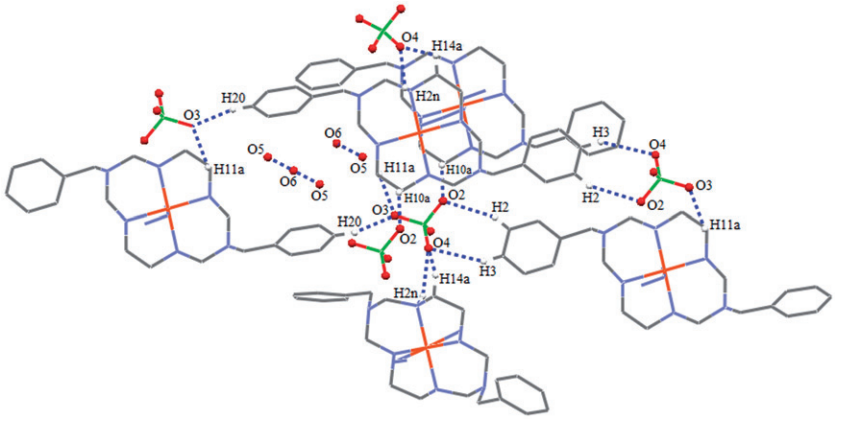

Figure 4. O···H hydrogen bonding by ClO_4^- and O···O and water(lattice)···water(lattice) hydrogen bonds. H (white) and O (red) (involving in H–bonding) are shown as small spheres of arbitrary radii.

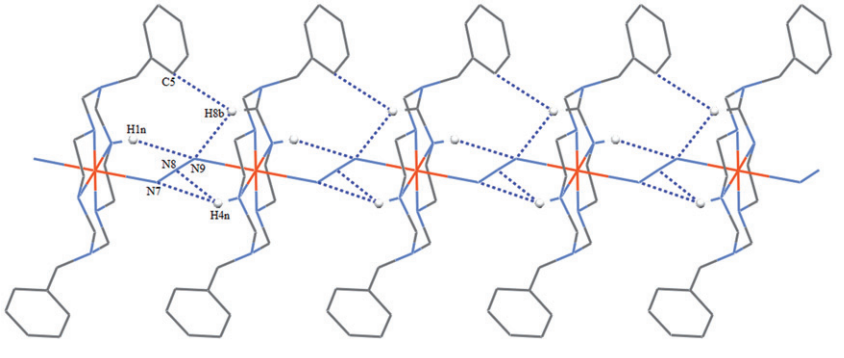

Figure 5. 1-D chain displaying N···H and C–H···π hydrogen bonding propagating along the *c*-axis. H (white) involved in H–bonding are shown as spheres of arbitrary radii.

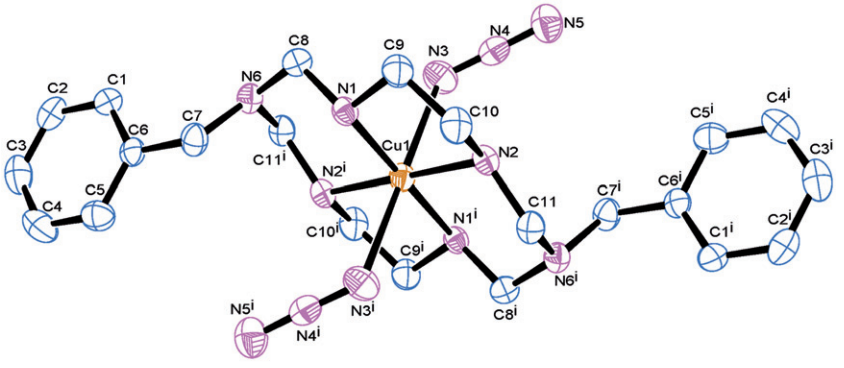

Figure 6. The molecular structure of **2** showing 30% probability displacement ellipsoids and atom-numbering scheme. Hydrogen atoms have been omitted for clarity.

Table 4. Bond lengths (Å) and angles (°) for **2**.

Bond lengths		Bond angles	
Cu(1)–N(1)	2.0127(19)	N(1)–Cu(1)–N(1)#1	180.0
Cu(1)–N(2)	2.0242(18)	N(2)–Cu(1)–N(2)#1	180.0
Cu(1)–N(3)	2.481(3)	N(1)–Cu(1)–N(2)	85.99(8)
N(4)–N(3)	1.181(3)	N(1)#1–Cu(1)–N(2)	94.01(8)
N(4)–N(5)	1.158(3)	N(1)–Cu(1)–N(3)	89.93(9)
		N(1)–Cu(1)–N(3)#1	90.06(9)
		N(2)–Cu(1)–N(3)	88.93(9)
		N(2)–Cu(1)–N(3)#1	91.08(9)
		Cu(1)–N(3)–N(4)	120.8(2)
		N(5)–N(4)–N(3)	178.7(3)
		C(11)#1–N(6)–C(8)	115.42(19)
		C(11)#1–N(6)–C(7)	115.92(18)
		C(8)–N(6)–C(7)	113.83(18)

Symmetry transformations used to generate equivalent atoms: #1: $-x, -y, -z+1$.

$[CuL(N_3)_2]$ crystallizes in the monoclinic $P2/1c$ space group. The asymmetric unit comprises half of the molecule and the other half is generated through a center of symmetry. The structure of **2** consists of one $[CuL]^{2+}$ and two azide counterions (figure 6). Each copper has axially distorted octahedral geometry and lies on a crystallographic inversion centre (figure 7). The coordination sphere around Cu(II) is similar to **1**. The $[CuL]^{2+}$ is bonded by two monodentate azides *trans* [38–40]. The equatorial Cu–N bond lengths are 2.0127(19)–2.0242(18) Å while *trans* N–Cu–N angles are 180° as required by symmetry. The *cis* N–Cu–N angles vary from 86.2(2) to 93.2(2)° for five-membered and six-membered chelate rings. The axial Cu(1)–N(3) bond is long (2.481(3) Å) and the azide is nearly linear (angle N(3)–N(4)–N(5) of 178.7(3)°).

The Cu(1)–N(3)–N(4) angle is 120.8(2)°. The Cu(1)–N(3) bond lies 88.9° from the equatorial plane suggesting that Cu(1)–N(3) is slightly bent off the perpendicular to the equatorial plane. Angles subtended at N(6) are 113.83(18)–115.92(18)° of the tertiary nitrogen atoms similar to **1**. Six-membered chelate rings adopt a chair conformation with a torsion angle of 57.97° whereas five-membered rings adopt a gauche conformation with a torsion angle of 55.77°. The crystal structure exhibits

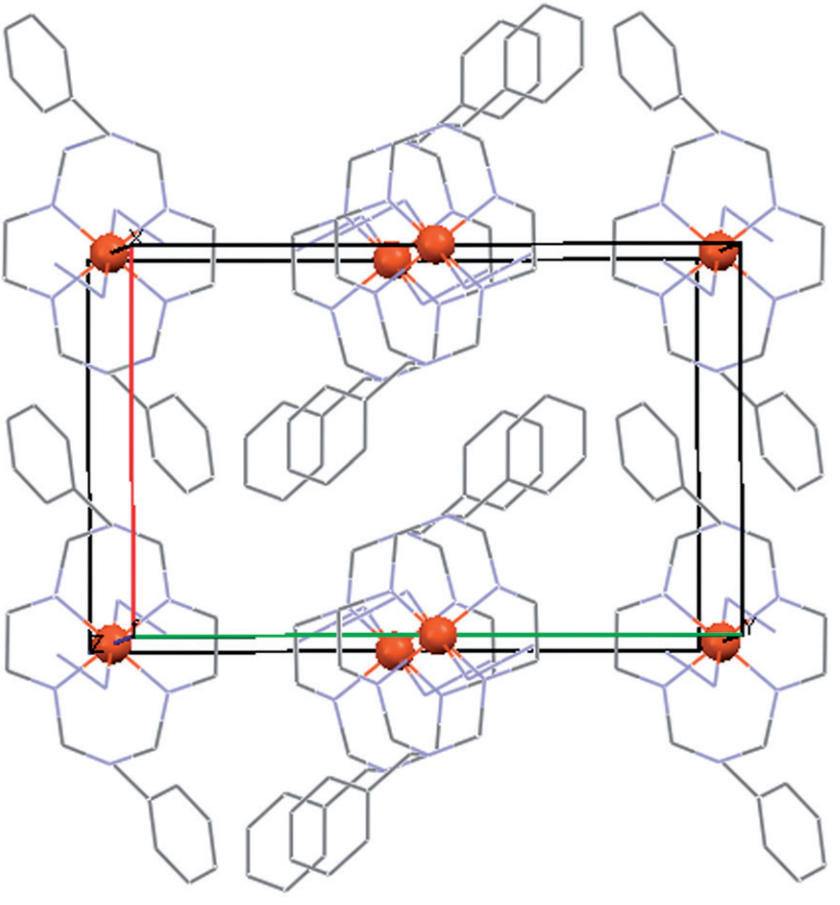

Figure 7. Unit cell diagram of **2** along the *c*-axis. Hydrogen atoms have been omitted for clarity. Cu (orange) are shown as spheres of arbitrary radii.

Table 5. Intramolecular and intermolecular hydrogen bonds, N–H···N, N–H···O, C–H···π and C–H···N, in **2**.

D–H–A	*d*(D···A) (Å)	*d*(H···A) (Å)	(D–H···A) (°)
N(1)–H(1N)···N(5)	3.153(3)	2.324(10)	160.8(19)
N(2)–H(2N)···N(4)	3.220(3)	2.53(3)	132.6(17) intramolecular
C(2)–H(2)···N(4)	3.483(6)	2.719(6)	139.88(6)
C(7)–H(7A)···π	3.685(5)	2.736(5)	165.98

N–H···N, C–H···N and C–H···π hydrogen bonding patterns (table 5). The H(1N) of the macrocycle ring is hydrogen bonded to the terminal nitrogen of azide [N(5)] of an adjacent molecule, forming a 12-membered ring (figure 8) with two Cu ions lying along the *c*-axis with a separation of 7.685 Å. C(7)–H(7A)···π hydrogen bond is observed giving stacking of aromatic rings in face-to-face mode leading to the formation of 1-D

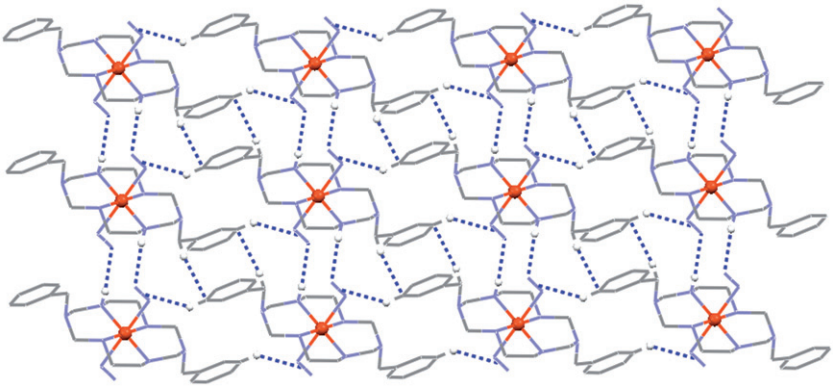

Figure 8. N···H and C–H···π hydrogen-bonded 2-D network of **2**. H (white) and Cu (orange) are shown as spheres of arbitrary radii.

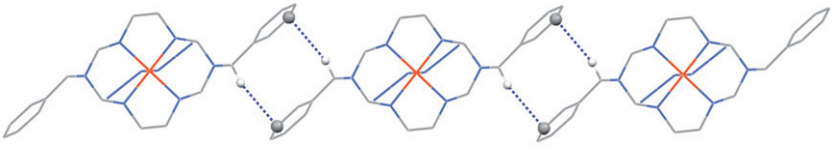

Figure 9. 1-D chain formed by C–H···π hydrogen bonds in **2**. H (grey) and C (dark grey) (involved in H-bonding) are shown as spheres of arbitrary radii.

chain (figures 8 and 9) with the shortest Cu···Cu distance equal to 12.963 Å [30]. N–H···N, C–H···N and C–H···π hydrogen bonding leads to a 3-D polymeric array (figure S1).

3.3. *Crystal structure description of* $[CuL^1N_3]_n \cdot [ClO_4]_n$ *(3)*

An ORTEP drawing of **3** with the atom numbering scheme is shown in figure 10. Crystallographic data, selected bond lengths and angles are listed in tables 1 and 6. $[CuL^1N_3]_n \cdot [ClO_4]_n$ crystallizes in the triclinic $P\bar{1}$ space group. The structure of **3** consists of $[CuL^1N_3]^+$ and ClO_4^- (figure 10). Each copper has an axially distorted octahedral geometry similar to **1** and **2** and lies on a crystallographic inversion centre (figure 11). The octahedron around Cu(II) is achieved by four secondary amine nitrogen atoms occupying the equatorial plane and the two terminal nitrogen atoms of the azide in axial positions. The $[CuL^1]^{2+}$ units are connected by bridging azides in the μ-1,3 (end-to-end) mode that brings two neighboring metal centers into a *trans*-position with respect to the azide, forming chains running along the *bc* plane, comprising a type-Iazido-bridged chain. The equatorial Cu–N bond lengths are 1.999(2)–2.018(2) Å and the *cis* N–Cu–N angles vary from 85.86(10)° to 94.14(10)° for five- and six-membered chelate rings. *Trans* N–Cu–N angles are 180°, the N(4)–N(3)–Cu(1) angle is 113.7(2)° and the N(1–2)–Cu(1)–N(3) bond angles are 88.72(10)–91.28(10)°, suggesting that the Cu(1)–N(3) linkage is slightly bent off the perpendicular to the equatorial plane.

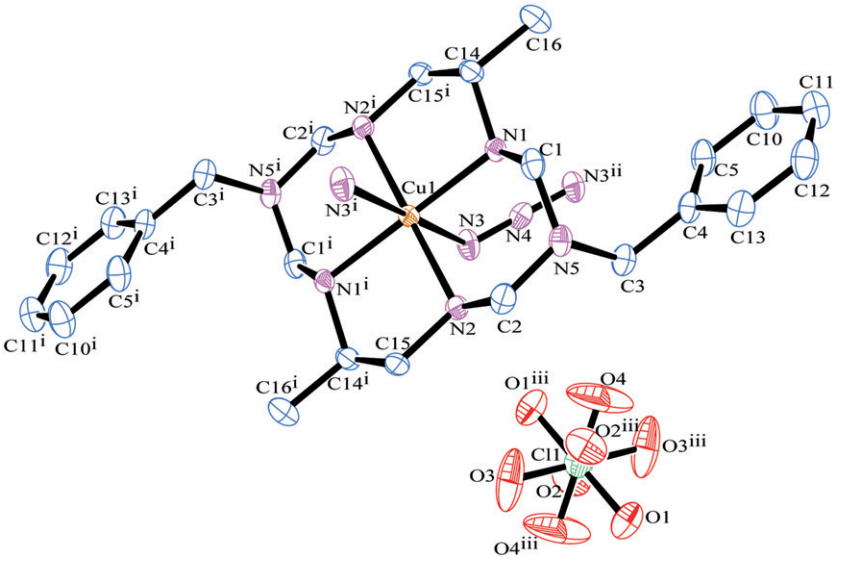

Figure 10. The molecular structure of **3** showing 30% probability displacement ellipsoids and atom-numbering scheme. Hydrogen atoms have been omitted for clarity.

Table 6. Bond lengths (Å) and angles (°) for **3**.

Bond lengths		Bond angles	
Cu(1)–N(1)#1	2.018(2)	N(1)–Cu(1)–N(3)	88.85(8)
Cu(1)–N(2)#1	2.000(2)	N(3)#2–N(4)–N(3)	180.0(2)
Cu(1)–N(3)	2.644(3)	N(4)–N(3)–Cu(1)	113.58(18)
N(4)–N(3)#2	1.175(2)	O(1)–Cl(1)–O(1)#3	180.0
N(1)–C(14)	1.488(3)	O(2)–Cl(1)–O(2)#3	180.0
N(1)–C(1)	1.499(3)	O(3)–Cl(1)–O(3)#3	179.999(1)
Cl(1)–O(1)#3	1.424(5)	O(4)–Cl(1)–O(4)#3	179.998(1)
Cl(1)–O(2)#3	1.533(5)	O(1)–Cl(1)–O(3)	107.5(4)
Cl(1)–O(3)#3	1.382(7)	O(1)–Cl(1)–O(2)	100.8(3)
Cl(1)–O(4)#3	1.277(8)	O(3)–Cl(1)–O(4)	118.1(7)
		O(4)–Cl(1)–O(1)	118.4(6)
Bond angles		O(4)–Cl(1)–O(2)	106.8(5)
N(1)#1–Cu(1)–N(1)	180.00(10)	O(3)–Cl(1)–O(2)	102.5(4)
N(2)#1–Cu(1)–N(2)	180.0	O(4)–Cl(1)–O(3)#3	61.9(7)
N(1)–Cu(1)–N(2)	94.18(9)	O(4)#3–Cl(1)–O(1)	61.6(6)
N(2)–Cu(1)–N(1)#1	85.82(9)	O(3)#3–Cl(1)–O(1)	72.5(4)
N(2)#1–Cu(1)–N(3)	91.35(9)	O(4)#3–Cl(1)–O(2)	73.2(5)
N(2)–Cu(1)–N(3)	88.65(9)	O(3)#3–Cl(1)–O(2)	77.5(4)
N(1)#1–Cu(1)–N(3)	91.15(8)	O(1)#3–Cl(1)–O(2)	79.2(3)

Symmetry transformations used to generate equivalent atoms: #1: $-x, -y+1, -z$; #2: $-x+1, -y+1, -z$; #3: $-x+1, -y, -z$.

Dihedral Cu–NNN–Cu torsion angle along the μ-1,3 azide bridge is 180°. The intrachain separation between two neighboring coppers along the chain is significantly longer at 6.59 Å.

Angles subtended at N(5) are 115.4(3)–115.6(2)° for tertiary nitrogen atoms. The six-membered chelate rings adopt a chair conformation with a torsion angle of 54.32°,

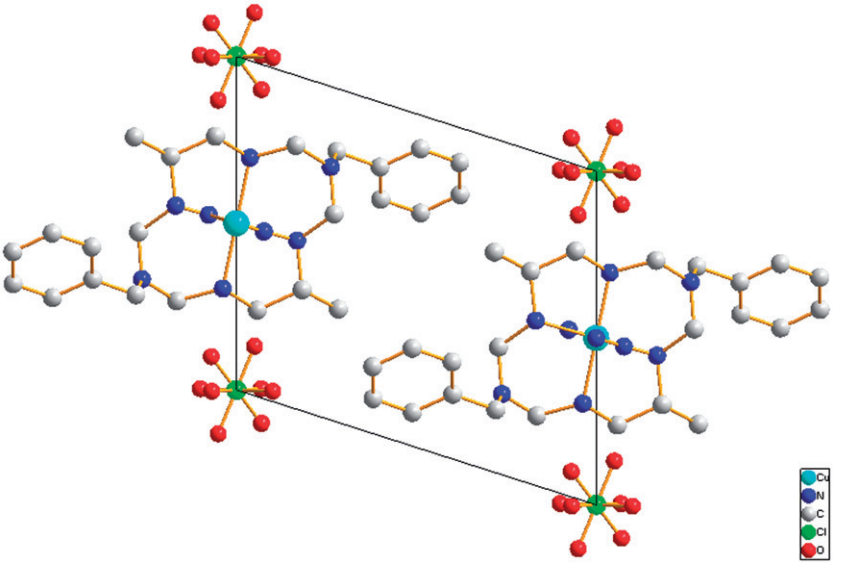

Figure 11. Unit cell diagram of **3** along the *b*-axis. Hydrogen atoms have been omitted for clarity.

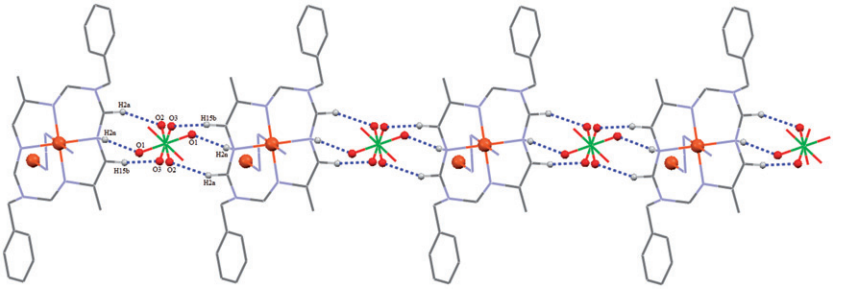

Figure 12. 1-D chain formed by N–H $\cdots$ N hydrogen bonds for **3**. H (grey) and O (red) are shown as spheres of arbitrary radii.

whereas five-membered rings assume a gauche conformation with a torsion angle of 53.60°. Bond distances in perchlorate Cl(1) vary from 1.341(9) to 1.537(6) Å. ClO_4^- ions fill up channels formed between the chains of octahedra and are held by hydrogen bonds (figures 12 and 13). They are stacked on top of each other in columns parallel to the *bc*-axis. Cl of ClO_4^- is situated at an inversion centre ($-x$, $-y$, $-z$). Azide nitrogen atoms N(3) and N(4) are intramolecularly hydrogen bonded to methylene hydrogen H(1B) and H(1N) of the secondary amine (table 7). H(3B) is engaged in hydrogen bonding (C–H $\cdots$ O) in bifurcated mode with the O(2) and O(1B) of perchlorate connecting two parallel running chains. O(1A) in the bifurcated mode is engaged in hydrogen bonding with H(2N) of coordinated amine and methylene H(15A), leading to the formation of a 2-D sheet (figure 13). All C–H $\cdots$ O, N–H $\cdots$ O, and C–H $\cdots$ N collectively form a 3-D supramolecular entity (figure 13). The shortest Cu $\cdots$ Cu distance between the two H-bonded chains is 10.102 Å.

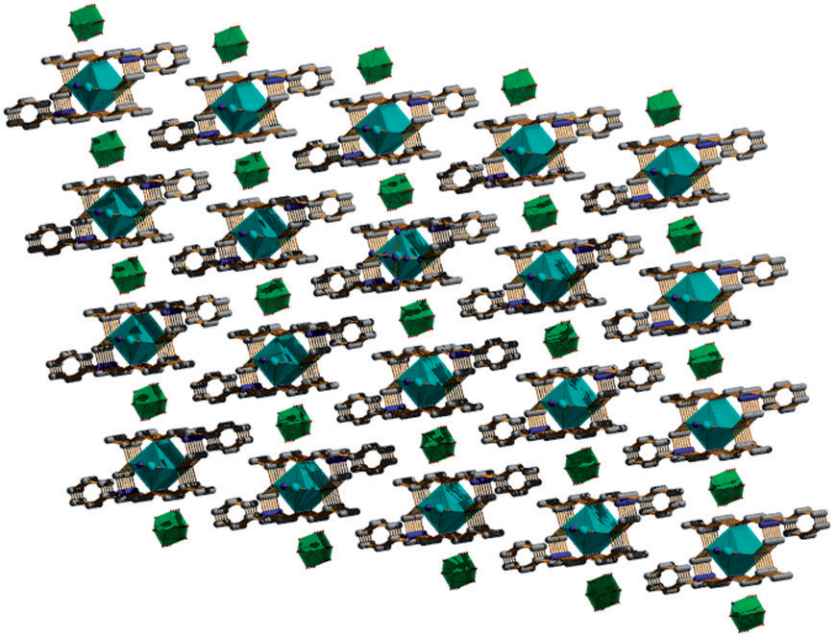

Figure 13. Polyhedral view of **3** along the *a*-axis.

Table 7. Intramolecular and intermolecular hydrogen bonds, N–H···N, N–H···O, C–H···N and C–H···O, in **3**.

D–H···A	*d*(D···A) (Å)	*d*(H···A) (Å)	(D–H···A) (°)
N(1)–H(1N)···N(4)	2.6900	3.215(2)	
N(2)–H(2N)···O(1)	2.33	3.115(6)	153
C(2)–H(2A)···O(2)	2.58	3.315(7)	133
C(15)–H(15B)···O(3)	2.47	3.233(10)	135

Oxygen atoms of perchlorate are severely disordered: O(1), O(2), O(3), and O(4) are symmetrically disordered over two positions with respect to the two-fold rotational symmetry, each with 50% occupation factor; while O(1) is disordered over two distinct sites with occupancies of 0.63(1) for O(1A) and 0.37(1) for O(1B). Both O(1A) and O(1B) are also symmetrically disordered over two positions with respect to the two-fold rotational symmetry.

3.4. *IR spectral studies*

IR spectra of **1**–**3** (figure S2) show characteristic absorptions of the hexaazamacrocyclic complexes at 3269–3194 cm^{-1}, indicating the presence of N–H groups. Several weak bands at 3050–2800 cm^{-1} are assigned to C–H stretches. The antisymmetric and symmetric stretching vibrations of azides, $\nu_{asym}(N_3)$ and $\nu_{sym}(N_3)$, can easily be

Table 8. EPR parameters of **1** and **3**.

Complex	Temperature	$g_{\|\|}$	$g_{\perp}$	g_{iso}	G	$A_{\|\|}$
$[CuLN_3]_n \cdot [ClO_4 \cdot 3/2H_2O]_n$ (**1**)	RT	2.109	2.07	2.083	1.576	.....
	LNT	2.178	2.068	2.104	2.674	161
$[CuL^1N_3]_n \cdot [ClO_4]_n$ (**3**)	RT	2.094	2.058	2.070	1.646	.....
	LNT	2.187	2.067	2.107	2.854	153.7

assigned. Bridging azides show a higher ν_{asym} and a lower ν_{sym} stretching mode than terminal azides [41]. The spectra of all complexes show a single strong band at 2063–2020 cm^{-1} corresponding to $\nu_{asym}(N_3)$ and medium intensity band at 1259–1272 cm^{-1} from the symmetric stretch. The characteristic deformation vibration of the azide $\delta(N_3)$ can be found at *ca* 627 cm^{-1} [42]. The stretching and bending modes of the C–C and C–N bonds have been observed between 1460–1360 cm^{-1} and 1270–750 cm^{-1}. The presence of uncoordinated perchlorate in **1** and **3** are inferred from the unsplit broad band around 1090 cm^{-1} (ν_3-antisymmetric stretching) and a band around 627 cm^{-1} (ν_4-antisymmetric bending) [43].

3.5. *EPR studies*

The X-band EPR spectra of polycrystalline powder of **1** and **3** were recorded at room temperature and in frozen acetonitrile : toluene (1 : 1) glass (figure S3) and EPR spectral parameters are summarized in table 8. The powder spectra at RT are typical of axial-type Cu(II) complexes with two g values, $g_{||} > g_{\perp} > 2.03$, suggesting a $d_{x^2-y^2}$ ground state, consistent with a tetragonally distorted octahedral stereochemistry [44]. The broadening of the spectrum of **3** is probably due to spin relaxation. The $g_{||} < 2.3$ indicates considerable covalent character [45, 46]. The smaller $g_{||}$ value indicates increased delocalization of the unpaired electron away from the metal and has been often interpreted in terms of increased covalency in the metal–ligand bond [47]. The calculated G value $[(g_{||} - 2.0023)/(g_{\perp} - 2.0023)] < 4$ (table 8) indicates some nuclear interaction [48].

The frozen solution spectra, axial with $g_{||} > g_{\perp} > 2.0$ and $G = 2.6$–2.9, suggest a square-based geometry of the complexes, as observed in the X-ray crystal structures. A square-based CuN_4 chromophore is expected to show $g_{||}$ of 2.200 and an $A_{||}$ of 150–165 G. The nuclear hyperfine coupling is observed in the $g_{||}$ signal with three of the four components clearly resolved, the last being obscured by $g_{\perp}$. Accordingly, the orbital ground state of Cu(II) would be basically $d_{x^2-y^2}$ and the polyhedra could be statistically distorted.

3.6. *Magnetic susceptibility studies*

Magnetization data were collected on all three compounds at 1.8 K in fields from 0 to 50 kOe. Magnetization of all samples show near saturation at 50 kOe at values near 6000 as expected for an $S = ½$ ion. No hysteresis was observed for the samples. Magnetic susceptibility data were collected from 1.8 to 310 K in an applied field of 1.0 kOe. Data for **1** are shown in figure 14. The $1/\chi$ data as a function of temperature are linear and yield a Weiss constant (θ) of zero within experimental error. The χT

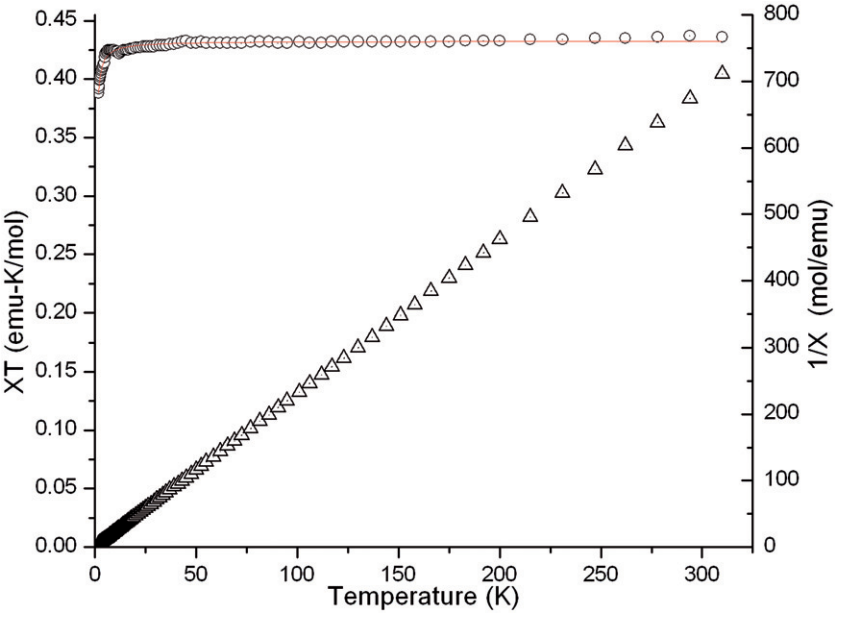

Figure 14. Temperature-dependant magnetic susceptibility data for **1**. Open circles are χT as a function of T (left axis) while open triangles show $1/\chi$ as a function of T (right axis). The solid line is the fit to the uniform Heisenberg $S = ½$ antiferromagnetic chain model.

data as a function of temperature were fit to the model for an $S = ½$ Heisenberg chain [49–52] (solid line in figure 14) yielding a Curie constant of 0.432 (2) emu-K mol^{-1} and an exchange constant of $J = -0.366(7)$ K, in agreement with the negligible Weiss constant. Similar magnetic behavior has been reported by Li *et al.* for $[Cu_2(\mu_{1,1}\text{-}N_3)_2(PP)_2)] \cdot 2ClO_4$ [53]. Compound **1** exhibits only very weak antiferromagnetic interactions while **2** and **3** show no sign of magnetic exchange (data for **3** shown in figure S4). The χT value is virtually constant over the entire temperature range at 0.42(1) emu-K mol^{-1} for **2** and 0.43(1) emu-K mol^{-1} for **3**.

4. Conclusion

Cu(II) complexes, having very similar macrocyclic blocking ligands and both azide and perchlorate as anions, have been synthesized. The use of building blocks forcing N_3^- to coordinate *trans* allowed us to tailor arrays of Cu(II) ions bridged by azides. Compound **1** exhibits only very weak antiferromagnetic interactions, while **2** and **3** show no signs of magnetic exchange, down to 1.8 K.

Supplementary material

Figures S1-S4 (Supplementary information) is available free of charge *via* the Internet at http://www.tandfonline.com/. Crystallographic data for the structural analysis have

been deposited with the Cambridge Crystallographic Data Centre, CCDC No. 814300 (**1**), 814301 (**2**), and 814302 (**3**). Copies of this information may be obtained free of charge from The Director, CCDC, 12 Union Road, Cambridge, CB21EZ, UK (Fax: +441223336033; E-mail: deposit@ccdc.cam.ac.uk or www.ccdc.cam.ac.uk/data request/cif).

Acknowledgments

We are indebted to the Department of Chemistry, IIT, Kanpur, and School of Chemistry, University of Hyderabad, for providing single-crystal X-ray facilities. A. Husain thanks the UGC Networking Resource Centre at the School of Chemistry, University of Hyderabad, for support under training visit program. We are grateful to the Council of Scientific and Industrial Research, New Delhi, (research scheme No. 21(0685)/07 EMR-II) for the financial support. S.A.A. Nami thanks the Department of Science & Technology for financial assistance under SERC FAST Scheme, No. SR/FT/CS-031/2008, New Delhi, India.

References

[1] S.R. Batten, R. Robson. *Angew. Chem. Int. Ed. Engl.*, **37**, 1460 (1998).
[2] B. Moulton, M.J. Zaworotko. *Chem. Rev.*, **101**, 1629 (2001).
[3] H. Abourahma, B. Moulton, V. Kravtsov, M.J. Zaworotko. *J. Am. Chem. Soc.*, **124**, 9990 (2002).
[4] S.R. Batten, R. Robson. *Angew. Chem. Int. Ed. Engl.*, **37**, 1460 (1998).
[5] S. Konar, P.S. Mukherjee, E. Zangrando, F. Lloret, N.R. Chaudhuri. *Angew. Chem. Int. Ed. Engl.*, **41**, 1561 (2002).
[6] Z.-L. You, H.-L. Zhu. *Z. Anorg. Allg. Chem.*, **632**, 140 (2006).
[7] P.S. Mukherjee, T.K. Maji, G. Mostafa, W. Hibbs, N.R. Chaudhuri. *New J. Chem.*, **25**, 760 (2001).
[8] P.S. Mukherjee, S. Dalai, G. Mostafa, T.-H. Lu, E. Rentschler, N.R. Chaudhuri. *New J. Chem.*, **25**, 1203 (2001).
[9] Y. Xie, Q. Liu, H. Jiang, C. Du, X. Xu, M. Yu, Y. Zhu. *New J. Chem.*, **26**, 176 (2002).
[10] M. Monfort, I. Resino, M.S. El Fallah, J. Ribas, X. Solans, M. Font-Bardia, H. Stoeckli-Evans. *Chem. Eur. J.*, **7**, 280 (2001).
[11] F. Meyer, H. Pritzkow. *Inorg. Chem. Commun.*, **4**, 305 (2001).
[12] J. Ribas, A. Escuer, M. Monfort, R. Vicente, R. Cortes, L. Lezama, T. Rojo. *Coord. Chem. Rev.*, **193**, 1027 (1999).
[13] A. Das, G.M. Rosair, M.S. El Fallah, J. Ribas, S. Mitra. *Inorg. Chem.*, **45**, 3301 (2006).
[14] E.-Q. Gao, A.-L. Cheng, Y.-X. Xu, M.-Y. He, C.-H. Yan. *Inorg. Chem.*, **44**, 8822 (2005).
[15] H.S. Yoo, J.I. Kim, N. Yang, E.K. Koh, J.-G. Park, C.S. Hong. *Inorg. Chem.*, **46**, 9054 (2007).
[16] X.-T. Liu, X.-Y. Wang, W.-X. Zhang, P. Cui, S. Gao. *Adv. Mater.*, **18**, 2852 (2006).
[17] Y.-Z. Zhang, H.-Y. Wei, F. Pan, Z.-M. Wang, Z.-D. Chen, S. Gao. *Angew. Chem. Int. Ed. Engl.*, **44**, 5841 (2005).
[18] T.-F. Liu, D. Fu, S. Gao, Y.-Z. Zhang, H.-L. Sun, G. Su, Y.-J. Liu. *J. Am. Chem. Soc.*, **125**, 13976 (2003).
[19] E.-Q. Gao, Y.-F. Yue, S.-Q. Bai, Z. He, C.-H. Yan. *J. Am. Chem. Soc.*, **126**, 1419 (2004).
[20] J.-P. Renard, L.-P. Regnault, M. Verdaguer. *Magnetism: Molecules and Materials*, p. 49, Wiley-VCH, Weinheim (2001).
[21] A. Caneschi, D. Gatteschi, N. Lalioti, C. Sangregorio, R. Sessoli, G. Venturi, A. Vindigni, A. Rettori, M.G. Pini, M.A. Novak. *Angew. Chem. Int. Ed. Engl. Engl.*, **40**, 1760 (2001).
[22] T. Kajiwara, M. Nakano, Y. Kaneko, S. Takaishi, T. Ito, M. Yamashita, A. Igashira-Kamiyama, H. Nojiri, Y. Ono, N. Kojima. *J. Am. Chem. Soc.*, **127**, 10150 (2005).
[23] A. Husain, A. Moheman, S.A.A. Nami, K.S. Siddiqi. *Inorg. Chim. Acta*, **384**, 309 (2012).
[24] A. Husain, S.A.A. Nami, K.S. Siddiqi. *Appl. Organomet. Chem.*, **25**, 761 (2011).

[25] *SMART & SAINT Software Reference Manuals*, Version 6.45; Bruker Analytical X-ray Systems, Inc., Madison, WI (2003).
[26] G.M. Sheldrick. *SADABS, Software for Empirical Absorption Correction, Ver. 2.05*, University of Göttingen, Germany (2002).
[27] *XPREP, 5.1 ed.*, Siemens Industrial Automation Inc., Madison, WI (1995).
[28] Oxford Diffraction. *CrysAlisPro (Version 171.31.8) and CrysAlis RED (Version 1.171.31.8)*, Oxford Diffraction Ltd, Abingdon, Oxfordshire, England (2007).
[29] *International Tables for Xray Crystallography, Vol. IV*, Kynoch Press, Birmingham, England (1974).
[30] G.M. Sheldrick. *SHELXL97, Program for Crystal Structure Refinement*, University of Göttingen, Germany (2008).
[31] L.J. Farrugia. *J. Appl. Cryst.*, **30**, 565 (1997).
[32] C.F. Macrae, P.R. Edgington, P. McCabe, E. Pidcock, G.P. Shields, R. Taylor, M. Towler, J. van de Streek. *J. Appl. Cryst.*, **39**, 453 (2006).
[33] K. Brandenburg, H. Putz. *DIAMOND, Version 3.0*, Crystal Impact GbR, Bonn, Germany (2005).
[34] R.L. Carlin. *Magnetochemistry*, Springer-Verlag, Berlin, Heidelberg, Germany (1986).
[35] A. Escuer, R. Vicente, M.S.E. Fallah, J. Ribas, X.J. Solans. *Dalton Trans.*, 2975 (1993).
[36] A. Escuer, R. Vicente, J. Ribas, M.S. El Fallah, X. Solans. *Inorg. Chem.*, **32**, 1033 (1993).
[37] S.-G. Kang, K. Ryu, S.-K. Jung, J. Kim. *Inorg. Chim. Acta*, **293**, 140 (1999).
[38] A.K. Chandra, T. Zeegers-Huyskens. *J. Phys. Chem. A*, **109**, 12006 (2005).
[39] L. Randaccio, M. Furlan, S. Geremia, M. Slouf. *Inorg. Chem.*, **37**, 5390 (1998).
[40] M.A.S. Goher, F.A. Mautner. *Transition Met. Chem.*, **24**, 693 (1999).
[41] L.F. Tang, H.Q. Shi, Z.H. Wang, L. Zhang. *J. Chem. Crystallogr.*, **30**, 159 (2000).
[42] B.-L. Li, X. Zhu, J.-H. Zhou, Y. Zhang. *Acta Cryst.*, **C60**, m373 (2004).
[43] T.M. Klapotke, K. Polborn, T. Schutt. *Z. Anorg. Allg. Chem.*, **626**, 1444 (2000).
[44] R. Cortes, M. Drillon, X. Solans, L. Lezama, T. Rojo. *Inorg. Chem.*, **36**, 677 (1997).
[45] S.S. Tandon, L.K. Thompson, J.N. Bridson, V. Mckee, A.J. Downard. *Inorg. Chem.*, **31**, 4635 (1992).
[46] D.F. Perkins, L.F. Lindoy, A. McAuley, G.V. Meehan, P. Turner. *Proc. Natl. Acad. Sci. U.S.A.*, **103**, 532 (2006).
[47] R.V. Gorkum, F. Buda, H. Kooijman, A.L. Spek, E. Bouwman, J. Reedijk. *Eur. J. Inorg. Chem.*, 2255 (2005).
[48] E. Garribba, G. Micera. *J. Chem. Edu.*, **83**, 1229 (2006).
[49] M. Cieplak, L.A. Turski. *J. Phys. C: Solid State Phys.*, **13**, L777 (1980).
[50] S. Ding, B. Guo, F. Su. *J. Math. Phys.*, **3**, 1153 (1999).
[51] J. Fivez. *J. Phys. C: Solid State Phys.*, **15**, 641 (1982).
[52] K.R. Reddy, M.V. Rajasekharan, J.-P. Tuchagues. *Inorg. Chem.*, **37**, 5978 (1998).
[53] H. Li, T.-T. Sun, S.-G. Zhang, J.-M. Shi. *J. Coord. Chem.*, **63**, 1531 (2010).